



On physical and data driven modelling of irrigation channels

Su Ki Ooi^{a,*}, M.P.M. Krutzen^b, E. Weyer^a

^a *Cooperative Research Centre for Sensor Signal and Information Processing, Department of Electrical and Electronic Engineering, The University of Melbourne, Parkville, VIC. 3010, Australia*

^b *DMP-Control Engineering Group, TNO Institute of Applied Physics, P.O. Box 155, 2600 AD DELFT, The Netherlands*

Received 21 May 2003; accepted 6 April 2004

Abstract

In this paper we test the St. Venant equations against real data in order to examine their accuracy and capability to describe the relevant dynamics of an irrigation channel. The St. Venant equations are simulated using the Preissmann scheme, and the simulated and real measured water levels are compared. Some of the parameters in the St. Venant equations are not exactly known and these parameters are also estimated from the observed data in order to improve the accuracy. Finally, a comparison with system identification models is performed in order to examine which model type is more suitable for control design and prediction purposes. The results show that the St. Venant equations can adequately capture the dynamics of real channels, and naturally, the model with estimated parameters is more accurate than the one with physical parameters. However, system identification models are as accurate as the St. Venant equations with estimated parameters, and they are preferred over the St. Venant equations for control and prediction purposes since they are much easier to use.

© 2004 Elsevier Ltd. All rights reserved.

Keywords: Modelling; System identification; Physical modelling; Parameter estimation; Environmental systems; Irrigation channel

1. Introduction

Due to the sharp rise in demand for water in many parts of the world, water is becoming an increasingly scarce resource (e.g. Jensen (1980)). It is not always the supply of water but the ability to fully and efficiently utilise the available quantities, which is the problem. It is therefore important to manage the water resources well and minimise the losses. This applies particularly to networks of irrigation channels, where large amounts of water are wasted due to poor management and control. These losses can be reduced by improving the decision support and control systems, and control of irrigation channels is an area which attracts increased attention, see e.g. Malaterre and Baume (1998) and the references therein, Malaterre (1998), Schuurmanns, Hof, Dijkstra,

Bosgra, and Brouwer (1999), Litrico (2002), de Halleux and Bastin (2002), Weyer (2002), Litrico and Pomet (2003), Litrico and Fromion (2003), Litrico, Fromion, Baume, and Rijo (2003), Ooi and Weyer (2003) and Weyer (2003). This is also evident from the special issue in January/February 1998 of *Journal of Irrigation and Drainage Engineering* on canal automation (Ano, 1998a), and the special sessions at the IEEE Systems, Man and Cybernetics conference in 1998 on modelling and control of water channels (Ano, 1998b).

In order to design a good controller or a decision support system, most design methods require a model that closely describes the relevant dynamics of the irrigation channel. Traditionally, the dynamics of an irrigation channel are modelled by the St. Venant equations (see, e.g. Cunge, Holly, & Verwey (1980), Chaudhry (1993) or French (1994)). The St. Venant equations are commonly used for prediction and control design for irrigation channels, see Malaterre and Baume (1998) for an overview. Despite widespread use, their accuracy are largely unknown which is surprising, taking into account the large amount of practically

*Corresponding author. Tel.: +61-383-446714; fax: +61-383-446678.

E-mail addresses: skoo@ee.mu.oz.au (Su Ki Ooi), krutzen@tpd.tno.nl (M.P.M. Krutzen), e.weyer@ee.mu.oz.au (E. Weyer).

oriented research which uses the St. Venant equations as a starting point. Hence, a natural question is therefore whether the St. Venant equations are capable of describing the relevant dynamics of an irrigation channel accurately? From laboratory experiments (Brutsaert, 1971), it is known that the St. Venant equations are an accurate representation of a small scale laboratory channel. To the authors' knowledge, only a few of the models based on the St. Venant equations (see, e.g. Rijo, Almeida, & Pereira (1992) and Litrico et al. (2003)) have been tested against data from real channels, which can be several kilometers long and the channel geometry is often nonuniform. In this paper, comparison of the St. Venant equations against real data is considered in order to examine their accuracy.

In addition, an equally important point is the accuracy of the boundaries conditions, that is the accuracy of the flow equations for the upstream and downstream gates. This is due to the fact that gate modelling and calibration of the flow equations are often difficult. Also, there is uncertainty in the friction slope equation because it is derived under idealistic assumptions (see, e.g. Chaudhry (1993)). Furthermore, the friction slope equation depends on the surface roughness (see e.g. Chaudhry (1993)) which is an approximate value since the real conditions of the channel will change with time and along the channel.

There are several different techniques that can be used to numerically solve the St. Venant equations, for example method of characteristics, finite element methods and finite difference methods (see e.g. Chaudhry (1993) and Roberson, Cassidy, & Chaudhry (1998)). The best known and most used finite difference method for solving the St. Venant equations is the Preissmann scheme (see e.g. Chaudhry (1993)). In order to examine the accuracy of the St. Venant equations, the water level in the channel is simulated using the Preissmann scheme and the simulated water level is compared against the measured water level. The unknown parameters in the St. Venant equations and the boundary conditions are estimated from the observed data, and the accuracy of the St. Venant equations with estimated and physical parameters is compared.

Previous works (see, e.g. Weyer (2001) and Ooi & Weyer (2001)) showed that good models for an irrigation channel can be obtained using system identification methods based on operational data from the channel. In those works, simple mathematical models that describe the dynamics of the channel adequately are identified using prediction error methods. The St. Venant equations are hyperbolic partial differential equations and much more complex than the system identification models, and it is an open question whether the St. Venant equations are significantly more accurate than the system identification models to justify their use. We therefore also compare the performance of the models based on the St. Venant equations and the

system identification models. In particular we examine their suitability for control design and prediction purposes.

The paper is organised as follows. In Section 2 a description of the irrigation channel is given. Then, in Section 3 the St. Venant equations are presented and the Preissmann scheme is briefly explained. The accuracy of the St. Venant equations and the boundary conditions are investigated in Section 4, followed by a comparison with system identification models in Section 5. Finally, conclusions are given in Section 6.

2. Channel description

The channel considered in this paper is the Haughton Main Channel (HMC) in Queensland, Australia. Fig. 1 shows a schematic side view of the channel. The channel is automated with overshot gates as shown in Fig. 1. As channels are located in rural areas, electric power is supplied by solar panels and data communication takes place via a radio network. We refer to the stretch of the channel between two gates as a pool. We name the pool according to the number of the upstream gate, e.g. the pools in Fig. 1 are Pools 9 and 10. y_9 , y_{10} and y_{11} are the upstream water level of gate 9, 10 and 11, respectively, and p_9 , p_{10} and p_{11} are the position of gate 9, 10 and 11. The amount of water above the gate is called the head over the gate, and denoted by h_9 , h_{10} and h_{11} .

The water levels, given in mAHD (meter Australia Height Datum), and the gate positions are the measured variables. Water levels are measured using submersible level pressure sensors and gate positions are measured based on the length of the steel cable between a gate and the motor that move the gate. The head over gate is computed from these variables. With reference to Fig. 1, the measured gate position

$$\bar{p} = p_{max} - p,$$

where p_{max} is the position when the gate is fully shut. Hence, a fully shut gate has measured position of 0 m and a positive value when the gate is open. The head over gate 9, 10 and 11 are calculated as

$$h_9 = y_9 + \bar{p}_9 - p_{max,9},$$

$$h_{10} = y_{10} + \bar{p}_{10} - p_{max,10},$$

$$h_{11} = y_{11} + \bar{p}_{11} - p_{max,11}.$$

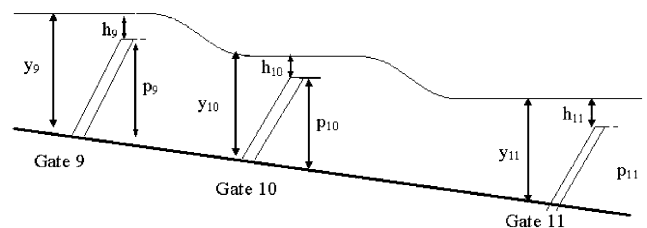


Fig. 1. Schematic of the channel with overshot gate 9, 10 and 11.

Due to variable communication delays and limits on the hardware processing capacity, the raw measurements of y and \bar{p} were collected with a nonuniform sampling interval of around 1 min. These measurements have been interpolated to achieve uniform sampling of 1 min and the unit of the water levels have been converted from mAHD to meter (the real water depth). There were virtually no differences in the plots of the raw data and the interpolated data, which was expected since the sampling intervals rarely deviated with more than a few seconds from 1 min.

3. St. Venant equations

The St. Venant equations are derived from a mass and momentum balance (e.g. Chaudhry (1993)) and are given by

$$\frac{\partial A}{\partial t} + \frac{\partial Q}{\partial x} = 0,$$

$$\frac{\partial Q}{\partial t} + \left(\frac{gA}{B} - \frac{Q^2}{A^2} \right) \frac{\partial A}{\partial x} + \frac{2Q}{A} \frac{\partial Q}{\partial x} + gA(S_f - \bar{S}) = 0. \quad (1)$$

The first equation in (1) is the mass balance, and it is sometimes also referred to as the continuity equation. The second equation is obtained from the momentum balance. A is the cross-sectional area of the channel, B is the width of the water surface, $g = 9.81 \text{ m/s}^2$ is the gravity, \bar{S} is the bottom slope, Q is the flow (discharge), and S_f is the friction slope. A commonly used relationship between the flow and the head over gate is $Q = ch^{3/2}$ (see, e.g. Bos (1978) or Chaudhry (1993)); where c is the gate constant. The gate constant of the upstream and downstream gate are labelled as c_{in} and c_{out} . For a sharp-edged rectangular channel, $c \approx 0.6\sqrt{gb}$ where b is the gate width (Fenton, 2001).

According to the Manning equation, in SI units

$$S_f = \frac{n^2 Q^2}{A^2 R^{4/3}}, \quad (2)$$

where n is the Manning coefficient, which mainly depends on the surface roughness. Table values of n for different surfaces are available (e.g. URL (2000)). $R = A/P$ is the hydraulic radius, where the wetted perimeter, P , is defined as the length of line of intersection of channel wetted surface with a cross-sectional plane normal to the flow (Chaudhry, 1993).

The pools we study are Pools 9 and 10 of the HMC. The physical data needed to solve the St. Venant equations numerically; like the length, bottom width, slope etc. (see Fig. 2), are given in Table 1.

The Manning coefficients are taken from (URL, 2000) for clean excavated earth channels. Obviously, the values listed in Table 1 are approximate since the real conditions of the channel will change with time and

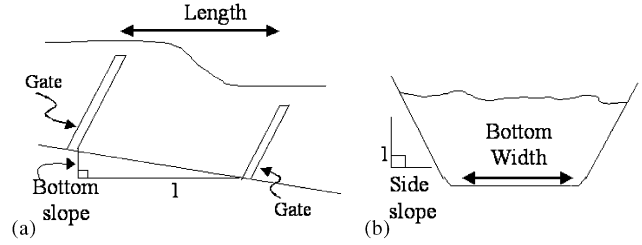


Fig. 2. (a) Side view of a channel. (b) Cross-section view of a channel.

Table 1
Physical data of Pools 9 and 10

	Pool 9	Pool 10
Length, L	853 m	3129 m
Bottom width, b_0	6 m	6 m
Side slope, s	2	2
Bottom slope	1.993×10^{-4}	9.907×10^{-5}
Gravity, g	9.81 m/s^2	9.81 m/s^2
Gate width, b	4.4 m	4.4 m
Manning coefficient, n	0.02	0.02
Upstream end gate constant, c_{in}	8.3	8.3
Downstream end gate constant, c_{out}	8.3	8.3

along the channel, and some parameters like the gate constant cannot be accurately measured or computed.

3.1. Preissmann scheme

Finite difference methods have been extensively used for simulation of complex dynamical systems, see, e.g. Chaudhry (1993). In these methods the time, t , and the spatial variable, x , are discretised into a grid on which the dynamical model is solved using approximations of the partial derivatives. The approximations are based on Taylor series expansions and are called explicit if the expansion is expressed in variables available at the current time instant. They are called implicit if the expressions involve future time instants. In the Preissmann scheme the functions, A and Q , and their partial derivatives are approximated as follows (note that all variables used in the St. Venant equations are in SI units):

$$A = \frac{1}{2}\alpha(A_{i+1}^{k+1} + A_i^{k+1}) + \frac{1}{2}(1-\alpha)(A_{i+1}^k + A_i^k),$$

$$\frac{\partial A}{\partial t} = \frac{(A_i^{k+1} + A_{i+1}^{k+1}) - (A_i^k + A_{i+1}^k)}{2\Delta t},$$

$$\frac{\partial A}{\partial x} = \frac{\alpha(A_{i+1}^{k+1} - A_i^{k+1})}{\Delta x} + \frac{(1-\alpha)(A_{i+1}^k - A_i^k)}{\Delta x},$$

$$Q = \frac{1}{2}\alpha(Q_{i+1}^{k+1} + Q_i^{k+1}) + \frac{1}{2}(1-\alpha)(Q_{i+1}^k + Q_i^k),$$

$$\frac{\partial Q}{\partial t} = \frac{(Q_i^{k+1} + Q_{i+1}^{k+1}) - (Q_i^k + Q_{i+1}^k)}{2\Delta t},$$

$$\frac{\partial Q}{\partial x} = \frac{\alpha(Q_{i+1}^{k+1} - Q_i^{k+1})}{\Delta x} + \frac{(1-\alpha)(Q_{i+1}^k - Q_i^k)}{\Delta x}.$$

Subscript i is the i th spatial grid point ($i = 1, \dots, M$) and superscript k is the k th time grid point ($k = 1, 2, \dots$), and Δx and Δt are the grid intervals along the x -axis and t -axis, and in this work we have used $\Delta x = 50$ m and $\Delta t = 60$ s. The parameter α is a weighting coefficient; the scheme is explicit if $\alpha = 0$ and totally implicit if $\alpha = 1$. The commonly used values are $0.6 \leq \alpha \leq 0.7$ (see Chaudhry (1993)), and in this paper we have used $\alpha = 0.6$.

Note that A can be expressed as $A = (b_0 + sy)y$, where b_0 is the bottom width of the channel and s is the side slope of the channel walls. Applying the above approximations for the partial derivatives to the St. Venant equation (1), two nonlinear algebraic equations are obtained. At any point in time, on each grid point there are two unknowns y_{i+1}^{k+1} and Q_{i+1}^{k+1} given that the solutions at the previous time and spatial grid points are available. Note that the initial values (i.e. at time $k = 1$) of the intermediate water levels within the pool are the solution of the St. Venant equations in steady state with the last spatial grid point equalling the measured water level. After the initial values are obtained, one solve for y_{i+1}^{k+1} and Q_{i+1}^{k+1} at the next point in time for all spatial grid points except for the first and last spatial grid points which correspond to the upstream and the downstream end. The above equations are augmented with boundary conditions at the upstream and downstream end. The boundary conditions are included directly in the system of equations. The upstream end boundary condition is

$$Q_{i=1}^{k+1} - Q_a^{k+1} = 0,$$

where $Q_a^{k+1} = c_{in}(h_{in}^{k+1})^{3/2}$ is the discretised inflow and h_{in}^{k+1} is the discretised head over upstream gate which is computed from the available measurements. The downstream end boundary condition is

$$Q_{i=M}^{k+1} = 0 \quad \text{if } h_{out}^{k+1} < 0,$$

$$Q_{i=M}^{k+1} = c_{out}(h_{out}^{k+1})^{3/2} \quad \text{otherwise,}$$

where $h_{out}^{k+1} = y_{i=M}^{k+1} - p_{max} + p_{out}^{k+1}$ is the discretised head over downstream gate, and p_{out}^{k+1} is the discretisation of the downstream gate opening which is equal to the measurement of the downstream gate position.

Using the boundary conditions, one also obtain the solution at the first and last spatial grid points. The procedure is then repeated for the next time point. Various iterative search techniques can be applied to solve the nonlinear algebraic equations, and the Newton-Raphson method (e.g. Kreyzig (1988)) is used in this paper.

4. Accuracy of the St. Venant's equations and the boundary conditions

In this section, the St. Venant equations are compared against real data. For Pool 9 two data sets are available. Data set 1 is collected under low flow, where the channel is operated at around 25% of its capacity, while data set 2 is collected at around 75% of channel capacity.

4.1. Pool 9

Data sets 1 and 2 for Pool 9 are plotted in Fig. 3. These figures show the position of gate 10 (\bar{p}_{10}), the head over gate 9 (h_9) and the water level upstream of gate 10 (y_{10}).

The gate constants and Manning coefficient in Table 1 are obtained based on approximate physical knowledge and are uncertain, hence these parameters, $\theta = [c_{in}, c_{out}, n]$ are also estimated using the observed data (see Krutzen (2000) for details). The estimation method used is a prediction error method with quadratic criterion, where the parameters are obtained by

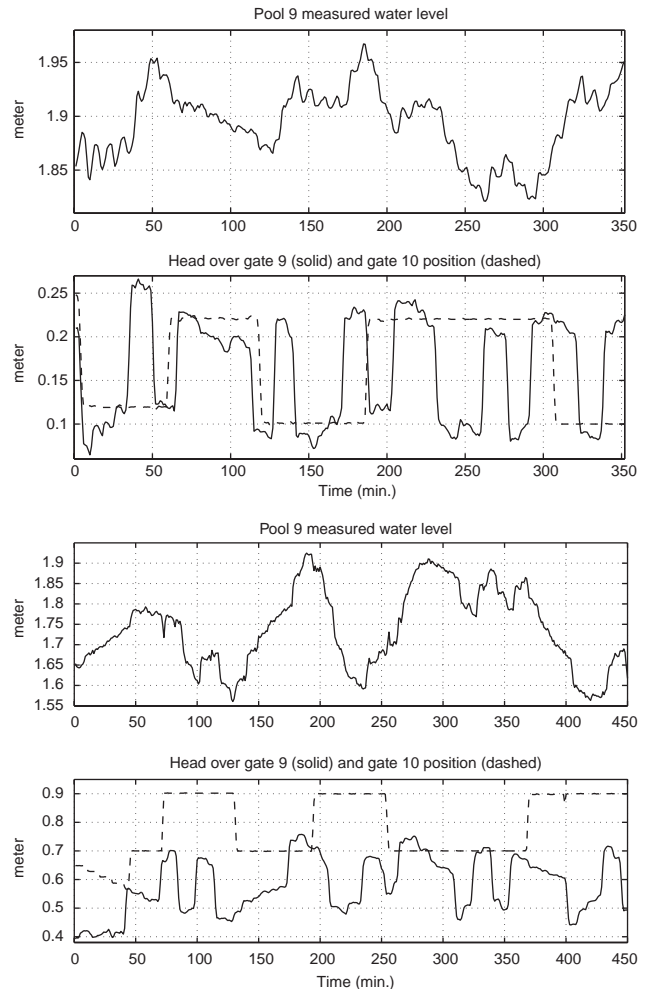


Fig. 3. Pool 9 data set 1 (top two plots) and 2 (bottom two plots): water level, y_{10} , and head over gate 9, h_9 and gate 10 position, \bar{p}_{10} .

minimising the sum of the squared prediction error, i.e. the criterion to be minimised (see e.g. Ljung (1999) or Söderström & Stoica (1988)) is

$$\frac{1}{N} \sum_{t=1}^N (\varepsilon(t, \theta))^2,$$

where N is the number data points, and the prediction error given by

$$\varepsilon(t, \theta) = y(t) - \hat{y}(t, \theta),$$

where $y(t)$ is the measured water level and $\hat{y}(t, \theta)$ is the simulated water level at the downstream end obtained by numerically solving the St. Venant equations. As the estimation of the parameters is a nonlinear least squares problem, an iterative search technique is used in order to find the solution (see e.g. Ljung (1999)). The Levenberg–Marquardt method (see Grace (1992) and the references therein) is used here. The first 200 data points of both data sets in Fig. 3 were used for estimation purposes and the rest were used for validation purposes. The estimated gate constants and Manning coefficients are given in Table 2. We next simulated the water level using the St. Venant equations and compared it to the measured one. As the first 200 data points are used for estimation purposes, the comparison is based on the validation set only. As mentioned in Section 3.1, the initial values of the intermediate water levels within the pool are the solution of the St. Venant equations in steady state with the water level at the last spatial grid point equalling the measured water level. However, it is clear from Fig. 3 that the channel is not in steady state at the start of the validation sets and one may try to start the simulation earlier and hope that at time 201 min the values of the intermediate water levels are approximately correct. However, this will cause the water level at the last spatial grid point to be different from the measured one at the time the comparison is started. Further investigations have shown that it is more important to have a correct initial water level for the last spatial grid point than approximately correct intermediate water levels. Hence, the simulation is performed by assuming steady-state initial condition, and the measured water level at time 201 min is used as the initial water level. The head over the upstream gate and the downstream gate position are used to calculate the boundary conditions. Investigations have shown that the effect of the initial conditions vanished reason-

Table 2
Estimated parameters of Pool 9

Estimated parameters	Measured data 1	Measured data 2
Manning coefficient, n	5.876×10^{-6}	2.022×10^{-2}
Upstream end gate constant, c_{in}	12.396	11.647
Downstream end gate constant, c_{out}	11.881	10.403

Table 3
Mean squared errors for Pool 9

Estimation set	Validation set	MSE (physical)	MSE (estimated)
Data set 1	Data set 1	1.077×10^{-4}	0.202×10^{-4}
Data set 2	Data set 2	11.11×10^{-4}	3.375×10^{-4}
Data set 1	Data set 2	—	4.690×10^{-4}
Data set 2	Data set 1	—	0.481×10^{-4}

ably fast. In fact the water levels simulated with different initial conditions are within 2 mm of each other in less than 80 min, and the MSE values reported in Table 3 do not change much with the initial conditions.

In addition to the standard validation, we also cross-validated by simulating data set 1 using the parameters estimated from data set 2 and vice-versa. Figs. 4 and 5 show the simulated and measured water levels for data set 1 and 2. The Mean Squared Error

$$\text{MSE} = \frac{1}{t_{end} - 199} \sum_{t=200}^{t_{end}} (y(t) - \hat{y}(t, \theta))^2 \quad (3)$$

between the measured and simulated water levels are given in Table 3. t_{end} is the final time instant of the validation set.

4.2. Pool 10

For Pool 10, we considered data collected under high flow as shown in Fig. 6.

As for Pool 9, the gate constants and the Manning coefficient are also estimated using a prediction error method. The first 200 data points in Fig. 6 are used for estimation purposes and the rest are used as the validation set. The estimated parameters are given in Table 4. The simulated and measured water levels are plotted in Fig. 7. The MSE between the simulated and measured water level are given in Table 5.

4.3. Discussion

There is good agreement between the Manning coefficient obtained from physical knowledge and the estimated ones, except when estimated using data set 1 for Pool 9, where the estimated Manning coefficient is very small. However, further investigations have shown that the simulated water level is insensitive to the value of the Manning coefficient for Pool 9. The gate constants estimated using measured data are similar to each other, but they are quite different from those computed based on physical data.

As expected, simulations using the St. Venant equations with estimated parameters give smaller MSE than with physical parameters and the simulated water levels also track the measured ones closer. Note that the

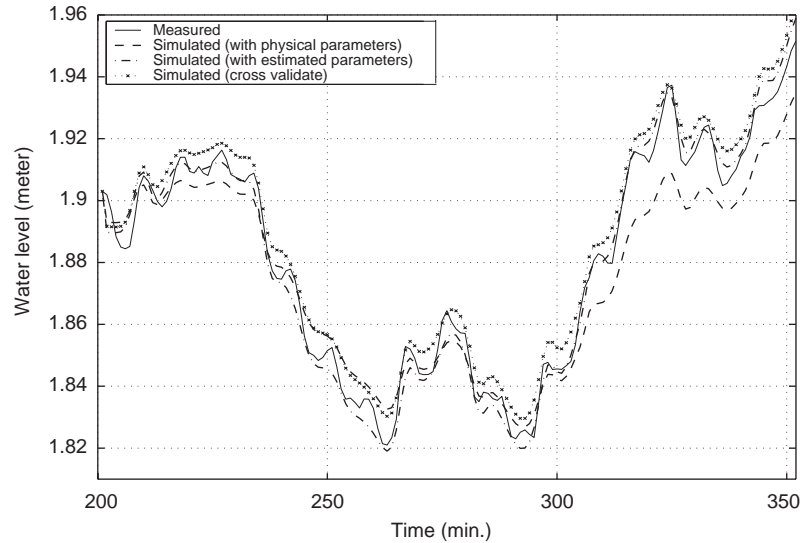


Fig. 4. Comparison of simulated and measured water levels of Pool 9 (Measured data 1).

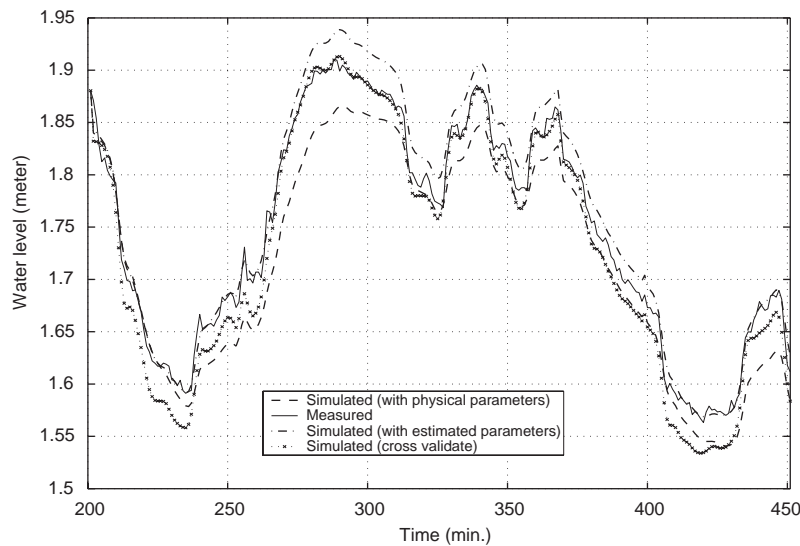


Fig. 5. Comparison of simulated and measured water levels of Pool 9 (Measured data 2).

improvement in accuracy is mainly due to the new values for the gate coefficients. That is, it is the boundary conditions for the St. Venant equations that have been improved. Also as expected, simulations using data from low flow conditions (data set 1) give smaller MSE than those from high flow conditions (data set 2). This is due to the fact that larger variations in water levels are expected under high flow conditions than under low flow conditions, and hence the model must track larger variations in the water level under high flow conditions.

In Pool 9, the St. Venant equations with physical parameters are able to capture the main trends and the waves in the water level but with an offset error. The

largest offset is around 3 cm and 6 cm for data set 1 and 2, respectively. As expected the performance is better with estimated parameters, where the models are able to accurately predict the water level with virtually no offset for data set 1, and with small errors of less than 4 cm over small time periods for data set 2. Pool 10 is much longer than Pool 9 and the models are not as accurate as for Pool 9 (larger MSE), and the largest offset is around 6 cm with physical parameters. The offset is smaller with estimated parameters, around 4 cm. Note that the models only have access to the initial water level, hence they are able to predict the water level ahead of time for at least $2\frac{1}{2}$ h. In a control setting the offsets can easily be corrected for by integral action in a feedback controller.

Therefore, apart from the offset, the St. Venant equations based purely on the physical data of the channel are able to capture the relevant dynamics, at least for control purposes.

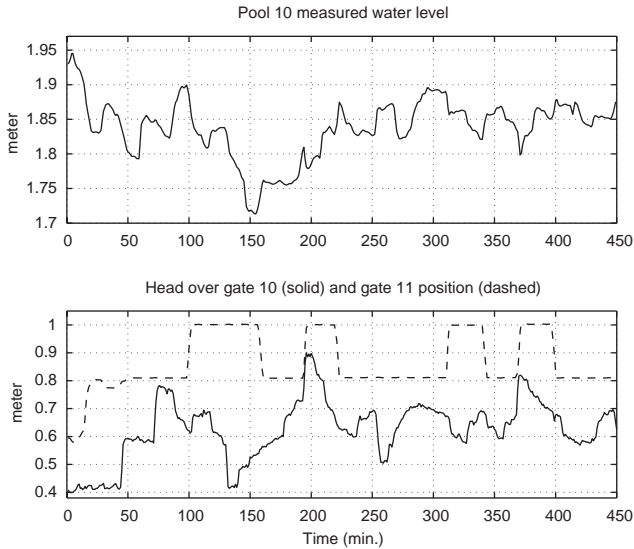


Fig. 6. Pool 10: water level, y_{11} (top), and head over gate 10, h_{10} and gate 11 position, \bar{p}_{11} (bottom).

Table 4
Estimated values of the Manning coefficient and the gate constants for Pool 10

Parameter	Estimate
Manning coefficient, n	1.848×10^{-2}
Upstream end gate constant, c_{in}	11.078
Downstream end gate constant, c_{out}	12.382

The reason for the drift in the simulated water level with physical parameters is probably due to the fact that the gate constants computed based on physical data are much smaller than those estimated. Hence, in this case the inflows and outflows are smaller than they should be, and this can cause a drift.

For Pool 9 we observe that after a period of discrepancy between the measured and simulated water levels (270–310 min) they converge again. This is due to the self correcting nature of the simulation models. If the simulated downstream water level is higher than the measured water level, then the simulated outflow is also higher than the actual outflow and the two water levels will approach each other. Similarly if the simulated water level is lower than the measured one.

5. Comparison with system identification models

In this section system identification models and the St. Venant equations are compared. From previous works [Weyer \(2001\)](#) and [Ooi and Weyer \(2001\)](#), it is known that a first-order nonlinear model is able to capture the main trends in the water level well and a third-order nonlinear model is able to give very accurate predictions of the water level several hours ahead. In addition, the third-order nonlinear model is also able to capture the waves in the water level, which are of course not

Table 5
Mean squared errors for Pool 10

MSE (physical parameters)	MSE (estimated parameters)
16.62×10^{-4}	3.996×10^{-4}

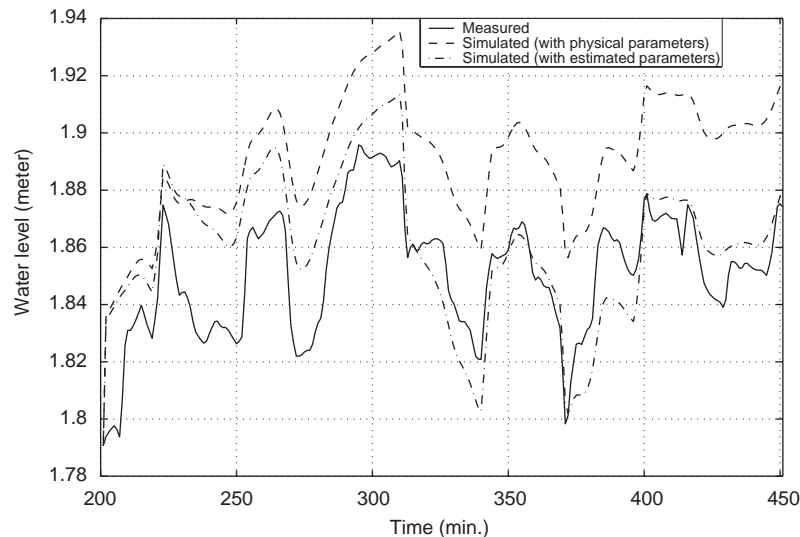


Fig. 7. Comparison of simulated and measured water levels of Pool 10.

captured by the first-order nonlinear model. The first- and third-order nonlinear models for pool i are shown in Eqs. (4) and (5).

$$y_{i+1}(t+1) = y_{i+1}(t) + c_{i,1}h_i^{3/2}(t-\tau) + c_{i+1,1}(y_{i+1}(t) + \bar{p}_{i+1}(t) - p_{max,i+1})^{3/2}, \quad (4)$$

$$\begin{aligned} y_{i+1}(t+1) = & c_{i,1}h_i^{3/2}(t-\tau) + c_{i,2}h_i^{3/2}(t-\tau-1) \\ & + c_{i,3}h_i^{3/2}(t-\tau-2) \\ & + c_{i+1,1}(y_{i+1}(t) + \bar{p}_{i+1}(t) - p_{max,i+1})^{3/2} \\ & + c_{i+1,2}(y_{i+1}(t-1) + \bar{p}_{i+1}(t-1) - p_{max,i+1})^{3/2} \\ & + c_{i+1,3}(y_{i+1}(t-2) + \bar{p}_{i+1}(t-2) - p_{max,i+1})^{3/2} \\ & + y_{i+1}(t) \\ & + \alpha_1(y_{i+1}(t) - 2y_{i+1}(t-1) \\ & + y_{i+1}(t-2)) + \alpha_2(y_{i+1}(t) - y_{i+1}(t-1)) \end{aligned} \quad (5)$$

y_{i+1} , h_i and \bar{p}_{i+1} are as defined in Section 2. τ is the time delay due to the time it takes for the water to travel from the upstream end to the downstream end of the channel.

The predictors associated with the first and third-order models for pool i are

$$\hat{y}_{i+1}(t+1, \theta) = \hat{y}_{i+1}(t, \theta) + c_{i,1}h_i^{3/2}(t-\tau) - c_{i+1,1}(\hat{y}_{i+1}(t, \theta) + \bar{p}_{i+1}(t) - p_{max,i+1})^{3/2}, \quad (6)$$

where $\theta = [c_{i,1}, c_{i+1,1}]$, and

$$\begin{aligned} \hat{y}_{i+1}(t+1, \theta) = & c_{i,1}h_i^{3/2}(t-\tau) + c_{i,2}h_i^{3/2}(t-\tau-1) \\ & + c_{i,3}h_i^{3/2}(t-\tau-2) \\ & + c_{i+1,1}(\hat{y}_{i+1}(t, \theta) + \bar{p}_{i+1}(t) \\ & - p_{max,i+1})^{3/2} \\ & + c_{i+1,2}(\hat{y}_{i+1}(t-1, \theta) + \bar{p}_{i+1}(t-1) - p_{max,i+1})^{3/2} \\ & + c_{i+1,3}(\hat{y}_{i+1}(t-2, \theta) + \bar{p}_{i+1}(t-2) \\ & - p_{max,i+1})^{3/2} + \hat{y}_{i+1}(t, \theta) \\ & + (\alpha_1)(\hat{y}_{i+1}(t, \theta) - 2\hat{y}_{i+1}(t-1, \theta) \\ & + \hat{y}_{i+1}(t-2, \theta)) \\ & + (\alpha_2)(\hat{y}_{i+1}(t, \theta) - \hat{y}_{i+1}(t-1, \theta)), \end{aligned} \quad (7)$$

where $\theta = [c_{i,1}, c_{i,2}, c_{i,3}, c_{i+1,1}, c_{i+1,2}, c_{i+1,3}, \alpha_1, \alpha_2]$. Note that the previously predicted water levels are used to predict future water levels in (6) and (7), i.e. the predictors are similar to the predictors associated with Output Error models in the linear case.

5.1. Pool 9

The unknown parameters, $\theta = [c_{9,1}, c_{10,1}]$ in the first-order nonlinear model, and $\theta = [c_{9,1}, c_{9,2}, c_{9,3}, c_{10,1}, c_{10,2}, c_{10,3}, \alpha_1, \alpha_2]$ in the third-order nonlinear model were obtained using system identification techniques (Weyer, 2001). The first 200 and 240 data points of data set 1 and

2, respectively were used for estimation purposes, and the rest were used for validation purposes. $\tau = 3$ was obtained using step test, see Weyer (2001), and the estimated parameters are shown in Table 6. The water level of the validation set is simulated using the St. Venant equations and the system identification models. The results are shown in Figs. 8 and 9 for data set 1 and 2, respectively (Note that predictors (6) and (7) are simulation models since they use the predicted water level at time t to predict the level at time $t+1$). The mean squared errors for the St. Venant equations (MSE St.V) and the system identification models (MSE SI) are given in Table 7. The MSE St.Vs are different from Table 3 since the simulations started at a different time instants.

5.2. Pool 10

The same procedure is repeated for Pool 10. The estimated parameters are given in Table 8 together with the time delay.

The measured, predicted and simulated water levels are shown in Fig. 10. The MSEs are given in Table 9.

5.3. Discussion

In Pool 9, the St. Venant equations with estimated parameters give the smallest MSE. However, the St. Venant equations with physical parameters are only as accurate as the first-order identification model, and the third-order nonlinear identification model gives smaller MSE than the St. Venant equations with physical parameters. In Pool 10, the model based on the St. Venant equations with physical parameters gives largest MSE, and the third-order identification model gives the smallest MSE.

Overall, there is not much difference in performance between the St. Venant equations with estimated parameters and the third-order nonlinear identification model, and both require observed data in order to find the parameters of the model. However, the third-order nonlinear model is much simpler to use for control and prediction purposes. Even a simple first-order model is good enough for control design (Weyer (2002, 2003)). In the event that a new automated control scheme is to be implemented in a channel where no operational data is available, then models based on the St. Venant equations must be used. The St. Venant equations also give the water levels at the intermediate grid points, while the identification models only give the downstream water level. However, models used for control design only needs to model the downstream water level, and if there are operational data available, the system identification models are as accurate as the St. Venant equations with estimated parameters and much easier to use for control design and prediction purposes.

Table 6
Pool 9 parameter estimates for first- and third-order nonlinear models

Data Set	Order	$c_{9,1}$	$c_{9,2}$	$c_{9,3}$	$c_{10,1}$	$c_{10,2}$	$c_{10,3}$	α_1	α_2
1	First	0.069	—	—	-0.063	—	—	—	—
2	First	0.070	—	—	-0.061	—	—	—	—
1	Third	0.137	-0.155	0.053	-0.190	0.333	-0.175	0.978	0.468
2	Third	0.150	-0.180	0.060	-0.172	0.264	-0.118	0.849	0.560

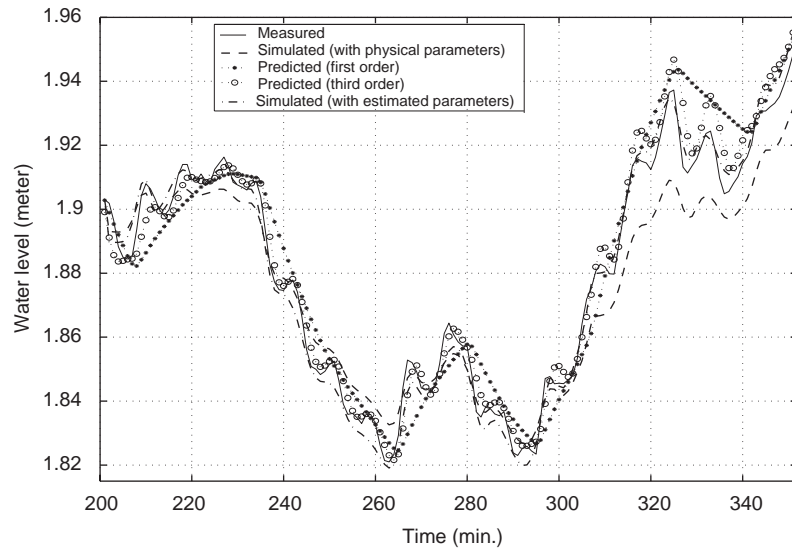


Fig. 8. Data set 1: The St. Venant equations, the system identification models and the measured water level in Pool 9.

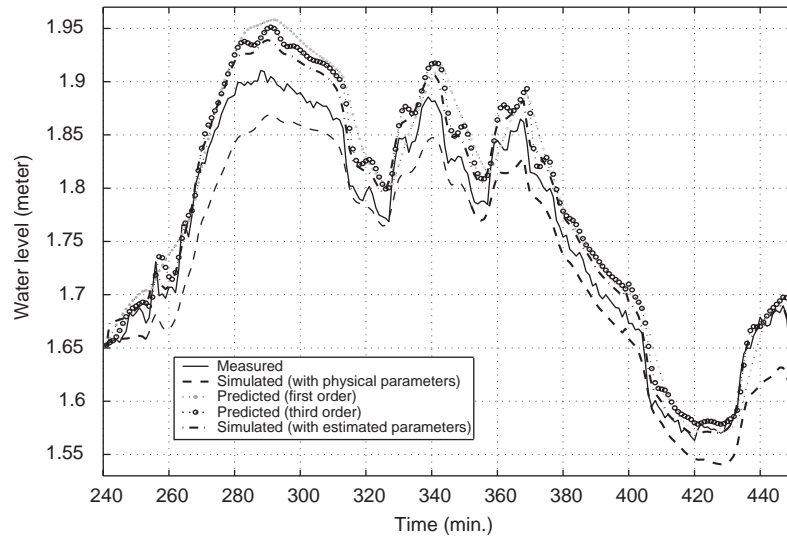


Fig. 9. Data set 2: The St. Venant equations, the system identification models and the measured water level in Pool 9.

Table 7
Pool 9 MSE of data set 1 (second row) and 2 (third row)

MSE St.V (physical)	MSE St.V (estimated)	MSE SI (first order)	MSE SI (third order)
1.077×10^{-4}	0.202×10^{-4}	1.107×10^{-4}	0.362×10^{-4}
10.15×10^{-4}	3.946×10^{-4}	11.652×10^{-4}	7.781×10^{-4}

6. Conclusion

In this paper the accuracy of the St. Venant equations is examined. Water levels simulated using the St. Venant equations with both physical and estimated parameters are compared against the measured water levels. The results show that the St. Venant equations can

Table 8
Pool 10 parameter estimates and time delays for first- and third-order nonlinear models

Order	$c_{10,1}$	$c_{10,2}$	$c_{10,3}$	$c_{11,1}$	$c_{11,2}$	$c_{11,3}$	α_1	α_2	Delay
First	0.0142	—	—	-0.0156	—	—	—	—	14 min
Third	0.134	-0.244	0.114	-0.101	0.185	-0.087	0.314	0.814	16 min

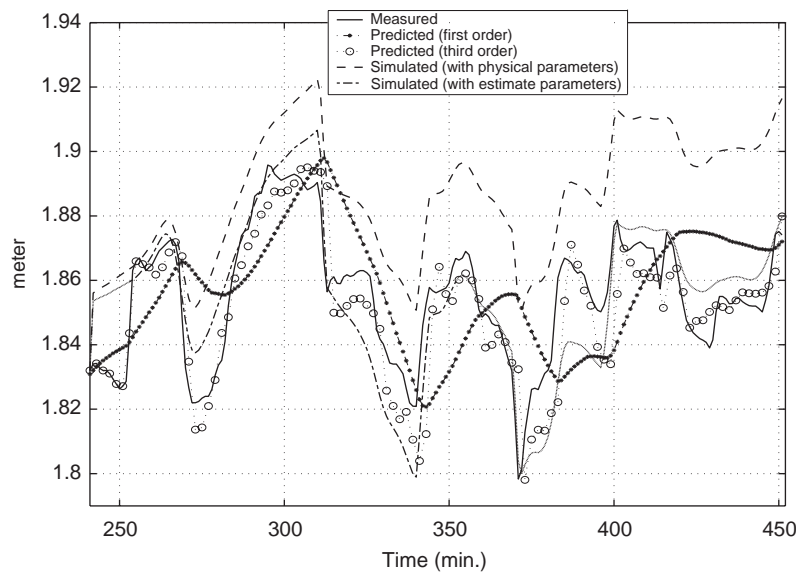


Fig. 10. The St. Venant equations, the system identification models and the measured water level of data set 2 in Pool 10.

Table 9
MSE of Pool 10

MSE St.V (physical)	MSE St.V (estimated)	MSE SI (first order)	MSE SI (third order)
11.00×10^{-4}	1.96×10^{-4}	4.44×10^{-4}	1.43×10^{-4}

adequately capture the dynamics of real open water channels. However, third-order nonlinear system identification models are as accurate as the St. Venant equations with estimated parameters and much simpler to use. Therefore, due to the complexity of the St. Venant equations, simple first- and third-order models obtained using system identification methods are preferred for control design and prediction purposes. Of course, if there is no operational data from the channel available then the St. Venant equations must be used. The St. Venant equations also give the water levels at the intermediate points along the channel, while the identification models only give the downstream water level. However, the downstream water level is all that is needed if the model is going to be used for control purposes. If there are operational data available, the system identification models are as accurate as the St. Venant equations with estimated parameters, and they are preferred since they are much easier to use for control design and prediction purposes.

Patent: A patent has been applied for to cover the developments that are described in this paper.

Acknowledgements

This research is part of a collaborative research project between the Department of Electrical and Electronic Engineering and Rubicon Systems on modelling and control of irrigation channels. The authors would like to thank Matthew Ryan at Rubicon System in Queensland for helping carrying out the identification experiments. They would also like to thank John Fenton and Iven Mareels for many fruitful discussions on modelling and simulation of irrigation channels. This work has been supported by Rubicon System Pty Ltd under the auspices of an AusIndustry Grant, and the Cooperative Research Centre for Sensor Signal and Information Processing under the Cooperative Research Centre scheme funded by The Commonwealth Government.

References

Ano. (1998a). *Journal of Irrigation and Drainage Engineering*, 124(1), 1–62.

- Ano. (1998b). *Proceedings of IEEE conference on system, man and cybernetics*, San Diego (pp. 1–62).
- Bos, M. (1978). *Discharge measurement structures*. International Institute for Land Reclamation and Improvement/ILRI, Wageningen, The Netherlands.
- Brutsaert, W. (1971). De Saint-Venant equations experimentally verified. *Journal of Hydraulic Division ASCE*, 97, 1387–1401.
- Chaudhry, M. H. (1993). *Open-channel flow*. Englewood Cliffs, NJ: Prentice-Hall.
- Cunge, J.A., Holly, F.M., & Verwey, A. (1980). *Practical aspects of computational river hydraulics*. Boston: Pitman Advanced Pub. Program.
- de Halleux, J., & Bastin, G. (2002). Stabilization of St. Venant equations using Riemann invariants: Application to waterways with mobile spillways. *Proceedings of 15th IFAC world congress*, Barcelona, Spain.
- Fenton, J.D. (2001). *River hydraulics (lecture note)*. The University of Melbourne (pp. 421–423).
- French, R. H. (1994). *Open-channel hydraulics*. New York: McGraw-Hill.
- Grace, A. (1992). *Optimization toolbox: For use with MATLAB*. The Math Works Inc., Natick, MA.
- Jensen, M.E. (1980). *Design and operation of farm irrigation systems*. ASAE Monograph No. 3. The American Society of Agricultural Engineers., St. Joseph, MI.
- Kreuzig, E. (1988). *Advanced engineering mathematics* (6th ed.). New York: Wiley.
- Krutzen, M. (2000). *Estimation of parameters in the St. Venant equations from observed data*. Internal Report, Department of Electrical and Electronic Engineering, The University of Melbourne, Australia.
- Litrico, X. (2002). Robust IMC flow control of SIMO dam-river open-channel systems. *IEEE Transactions on Control Systems Technology*, 10(3), 432–437.
- Litrico, X., & Fromion, V. (2003). Advanced control politics and optimal performance for an irrigation canal. *Proceedings of the 2003 European control conference*, Cambridge, UK.
- Litrico, X., Fromion, V., Baume, J.-P., & Rijo, M. (2003). Modelling and PI control of an irrigation canal. *Proceedings of the 2003 European control conference*, Cambridge, UK.
- Litrico, X., & Pomet, J.-B. (2003). Nonlinear modelling and control of a long river stretch. *Proceedings of the 2003 European control conference*, Cambridge, UK.
- Ljung, L. (1999). *System identification: Theory for the user* (2nd ed.). Englewood Cliffs, NJ: Prentice-Hall.
- Malaterre, P. O. (1998). PILOTE: Linear quadratic optimal controller for irrigation canals. *Journal of Irrigation and Drainage Engineering*, 124(4), 187–194.
- Malaterre, P.-O., & Baume, J.-P. 1998. Modeling and regulation of irrigation canals: Existing applications and ongoing researches. *IEEE international conference on systems, man and cybernetics*, San Diego, CA (pp. 3850–3855).
- Ooi, S.K., & Weyer, E. (2001). Closed loop identification of an irrigation channel. *Proceedings of the 40th IEEE CDC*, Orlando, USA (pp. 4338–4343).
- Ooi, S.K., & Weyer, E. (2003). Control design for an irrigation channel from physical data. *Proceedings of the 2003 European control conference*, Cambridge, UK.
- Rijo, M., Almeida, A.B., & Pereira, L.S. (1992). Mathematical modelling and field study of unsteady flow in an irrigation canal. *Proceedings of the fourth international conference on hydraulic engineering software*, Valencia (pp. 339–349).
- Roberson, J. A., Cassidy, J. J., & Chaudhry, M. H. (1998). *Hydraulics engineering* (2nd ed.). New York: Wiley.
- Schuermans, J., Hof, A., Dijkstra, S., Bosgra, O., & Brouwer, R. (1999). Simple water level controller for irrigation and drainage canals. *Journal of Irrigation and Drainage Engineering*, 125(4), 189–195.
- Söderström, T., & Stoica, P. (1988). *System identification*. Englewood Cliffs, NJ: Prentice-Hall.
- URL. (2000). <http://www.lmnoeng.com/manningn.htm>. LMNO engineering, research, and software, Ltd., Athens, Ohio, USA.
- Weyer, E. (2001). System identification of an open water channel. *Control Engineering Practise*, 9, 1289–1299.
- Weyer, E. (2002). Decentralised PI controller of an open water channel. *Proceedings of the 15th IFAC world congress*, Barcelona, Spain.
- Weyer, E. (2003). LQ control of an irrigation channel. *Proceedings of the 42nd IEEE conference on decision and control*, Hawaii, USA, (pp. 750–755).